



저작자표시-비영리-변경금지 2.0 대한민국

이용자는 아래의 조건을 따르는 경우에 한하여 자유롭게

- 이 저작물을 복제, 배포, 전송, 전시, 공연 및 방송할 수 있습니다.

다음과 같은 조건을 따라야 합니다:



저작자표시. 귀하는 원저작자를 표시하여야 합니다.



비영리. 귀하는 이 저작물을 영리 목적으로 이용할 수 없습니다.



변경금지. 귀하는 이 저작물을 개작, 변형 또는 가공할 수 없습니다.

- 귀하는, 이 저작물의 재이용이나 배포의 경우, 이 저작물에 적용된 이용허락조건을 명확하게 나타내어야 합니다.
- 저작권자로부터 별도의 허가를 받으면 이러한 조건들은 적용되지 않습니다.

저작권법에 따른 이용자의 권리는 위의 내용에 의하여 영향을 받지 않습니다.

이것은 [이용허락규약\(Legal Code\)](#)을 이해하기 쉽게 요약한 것입니다.

[Disclaimer](#)

Master's Thesis  
석사 학위논문

# Synthesis of doped ZnS Nanostructures

Mansoo Park ( 박 만 수 朴 萬 洙 )

Department of Emerging Materials Science

신물질과학전공

**DGIST**

**2017**

Master's Thesis  
석사 학위논문

# Synthesis of doped ZnS Nanostructures

Mansoo Park ( 박 만 수 朴 萬 洙 )

Department of Emerging Materials Science

신물질과학전공

**DGIST**

**2017**

# Synthesis of doped ZnS Nanostructures

Advisor : Professor Jung-Il Hong

Co-Advisor : Dr. Soon Moon Jeong

by

Mansoo Park

Department of Emerging Materials Science

DGIST

A thesis submitted to the faculty of DGIST in partial fulfillment of the requirements for the degree of Master of Science in the Department of Emerging Material Science. The study was conducted in accordance with Code of Research Ethics<sup>1</sup>

06. 27. 2016

Approved by

Professor Jung-Il Hong ( Signature )  
(Advisor)

Dr. Soon Moon Jeong ( Signature )  
(Co-Advisor)

---

<sup>1</sup> Declaration of Ethical Conduct in Research: I, as a graduate student of DGIST, hereby declare that I have not committed any acts that may damage the credibility of my research. These include, but are not limited to: falsification, thesis written by someone else, distortion of research findings or plagiarism. I affirm that my thesis contains honest conclusions based on my own careful research under the guidance of my thesis advisor.

# Synthesis of doped ZnS Nanostructures

Mansoo Park

Accepted in partial fulfillment of the requirements for the degree of Master of Science.

06. 27. 2016

Head of Committee 홍 정 일 (인)

Prof. Jung-Il Hong

Committee Member 정 순 문 (인)

Dr. Soon Moon Jeong

Committee Member 서 정 필 (인)

Prof. Jungpil Seo

## Abstract

Zinc Sulfide (ZnS) is one of the most widely used  $\text{II-VI}$  inorganic semiconductor materials with a direct wide bandgap of 3.77eV for wurtzite phase and 3.72eV for cubic phase. Due to their excellent luminescence and physical properties, they have been used for sensors, light emitting diodes (LEDs) and lasers. In this regard, many researchers have tried to synthesize one-dimensional (1D) ZnS nanostructures, such as nanorods, nanowires, nanobelts, nanoribbons and nanotubes. In the present work, we have studied the 1D ZnS nanostructures prepared at various growth temperatures employing thermal chemical vapor deposition (Thermal CVD) system. The powder of zinc sulfide (ZnS), copper (Cu) and manganese (Mn) were used as the starting material and gold (Au) thin films were introduced as the catalytic promoter for the growth of nanowires. In this thermal evaporation process, the reaction temperature and starting materials played crucial roles for the formation of 1D ZnS nanostructures. The growth temperature and starting materials were found to be the main factors to define the morphology of the 1D ZnS nanostructures. The morphology, element analysis and phase structure were studied using high-resolution field emission scanning electron microscopy (HR FE-SEM), and x-ray diffraction (XRD). The XRD confirmed the phase present in the ZnS. The luminescence properties of 1D ZnS nanostructures were investigated by cathodoluminescence (CL) system.

Keywords: Zinc sulfide, One dimensional materials, Doping, Thermal Chemical vapor deposition

# Contents

<b>Abstract</b> .....	<b>i</b>
<b>Contents</b> .....	<b>ii</b>
<b>List of tables</b> .....	<b>iii</b>
<b>List of figures</b> .....	<b>iv</b>
<b>I. Introduction</b> .....	<b>1</b>
1.1 Motivation.....	1
1.2 Literature reviews .....	8
<b>II. EXPERIMENTAL DETAILS</b> .....	<b>10</b>
2.1 Synthesis of ZnS nanostructures .....	10
2.1.1 Chemical vapor deposition .....	10
2.2 Experimental method.....	13
2.2.1 Experimental materials .....	13
2.2.2 Preparation of catalytic layer on substrate.....	13
2.2.3 Synthesis of un-doped / doped ZnS nanostructures.....	16
2.3 Characterizations .....	19
2.3.1 X-ray diffraction (XRD).....	19
2.3.2 Electron microscopy (EM) .....	21
2.3.3 Cathodoluminescence (CL) .....	25
<b>III. RESULT AND DISCUSSION</b> .....	<b>26</b>
3.1 Deposit rate of the Au catalytic layer.....	26
3.2 Morphology .....	26
3.3 Structural properties.....	31
3.4 Luminescence properties .....	33
<b>IV. CONCLUSIONS</b> .....	<b>36</b>
<b>References</b> .....	<b>37</b>

**Summary (in Korean) ..... 45**

**List of tables**

Table I. Substrate preparation procedure. .... 14

Table II. Experimental condition for various temperatures. .... 17

Table III. Experimental condition for various doping materials..... 17

## List of figures

Figure 1.1 Top: Sixteen emission colors from small (blue) to large (red) CdSe Qdots excited by a near-ultraviolet lamp; size of Qdots can be from ~1 nm to ~10 nm. Bottom: Photoluminescence spectra of some of the CdSe Qdots .	3
Figure 1.2 Classification of nanostructures based on demensionlity. ....	4
Figure 1.3 Optical characteristics of the wind-driven ML. (a) Schematic illustration of the set-up. (b) Photograph of the ML image. (c-f) Photographs obtained from wind-driven ML.. ....	7
Figure 1.4 (a) The zinc blende and (b) wurtzite structures. The Yellow represents the sulfur atoms and gray represents the zinc atoms.....	9
Figure 2.1 (a) SEM image of ZnS nanowire bundles grown on a CdSe substrate that was first deposited on Si(111). The CdSe is a solid film, but the ZnS is a bundle of aligned nanowires. (b) Enlarged SEM image of a ZnS bundle showing traces created due to fluctuation in growth condition, presenting the equal growth rate of all of the nanowires. (c) Fractured surface of the sample showing the direct growth of ZnS nanowires on the CdSe crystals and the preservation in the ZnS nanowire bundles of the surface morphology of the CdSe crystal. (d) Enlarged top view of the aligned ZnS nanowires.....	12
Figure 2.2 Schematic of the DC magnetron sputtering system.....	15

Figure 2.3 (a) The schematic set up of Thermal CVD system and (b) synthesis process of the 1D ZnS nanostructures with Thermal CVD. (c) Temperature profile of the furnace .....	18
Figure 2.4 Diffraction of x-rays by a crystal.....	20
Figure 2.5 Schematic diagram of scanning electron microscope.....	23
Figure 2.6 Interaction of the electron beam with the sample; Signal generated when an electron beam is incident on a sample.....	24
Figure 3.1 Scanning electron microscopy images showing different morphologies of un-doped 1D ZnS structures synthesized with different set of temperature: (a-b) 900 °C, (c-d) 1000 °C, and (e-f) 1200 °C. Insert is the side-view EM image of the Y-shaped ZnS belts.. ..	29
Figure 3.2 Scanning electron microscopy images showing different morphologies of transition metal doped 1D ZnS nanostructures synthesized with different dopant species (a-b) none, (c-d) Cu, and (e-f) Mn. Insert is the low magnification EM image of the (a) ZnS, (c) ZnS:Cu, and (e) ZnS:Mn NWs respectively.....	30
Figure 3.3 XRD pattern of synthesized products of (a) un-doped, (b) Cu doped, and (c) Mn doped ZnS nanostructures. And XRD pattern of ICSD reference files of cubic and hexagonal phased ZnS. ....	32
Figure 3.4 Room temperature CL Spectra of (a) un-doped, (b) Cu, and (c) Mn doped 1D ZnS nanostructures.....	36

# I. Introduction

## 1.1 Motivation

In the past decade, the science and technology have evolved toward the precise control of material structures in nanometer scale, developing the field of nanotechnology. Nanostructures are usually defined as a structures having at least one dimension (D) in the 1 ~ 100nm size range.<sup>1,2</sup> When the size of material reduces to the critical value called Bohr radius, the electron energy level stops overlapping with each other and shows quantized energy band.<sup>3</sup> Resulting in nanostructures exhibiting unique properties originating from their size dependent effects such as quantum confinement effect that cannot be recognized not observed in bulk materials.<sup>2,4,5,6,7</sup> For example, Bawendi et al. showed the color change of CdE (E = S, Se, Te) semiconductor nanocrystals depending on their sizes,<sup>8</sup> where the color reflects the magnitudes of band gaps in the nanocrystals. Figure 1.1 shows that change of photoluminescence spectra changes depending on the size of CdSe quantum dots. When the quantum dot diameter is reduced, a blue shift of the band gap energy is usually observed.<sup>23</sup> Additionally, nanostructures have been shown to exhibit a different thermal stability which depending on the particles size.<sup>9,10</sup> Hong et al. found that extremely thin ZnO nanoplates may exhibit magnetism even at room temperature.<sup>11</sup>

Figure 1.2 shows classification of nanomaterials according to their dimensions; 0D, 1D and 2D nanostructures. 0D nanostructures includes nanocrystals,<sup>12</sup> nanospheres,<sup>13</sup> and quantum dots<sup>14</sup> whose size are in nanometer scales in all three dimensions.<sup>2,15</sup> 1D nanostructures such as nanowires,<sup>16</sup> and nanotubes<sup>17</sup> are non-nanoscaled linear structures whose size is in nm scale in only one dimension. 2D nanostructures, including nanoplates,<sup>18</sup> and nanosheets,<sup>19</sup> are non-nanoscaled in two dimensions. These nanostructures have been evaluated as excellent systems to study thermal, electrical and optical properties corresponding to their sizes. In particular, 1D nanostructures are expected to be used for optoelectric and semiconductor devices such as display,<sup>20</sup> biosensors,<sup>21</sup> and transistor.<sup>22</sup>

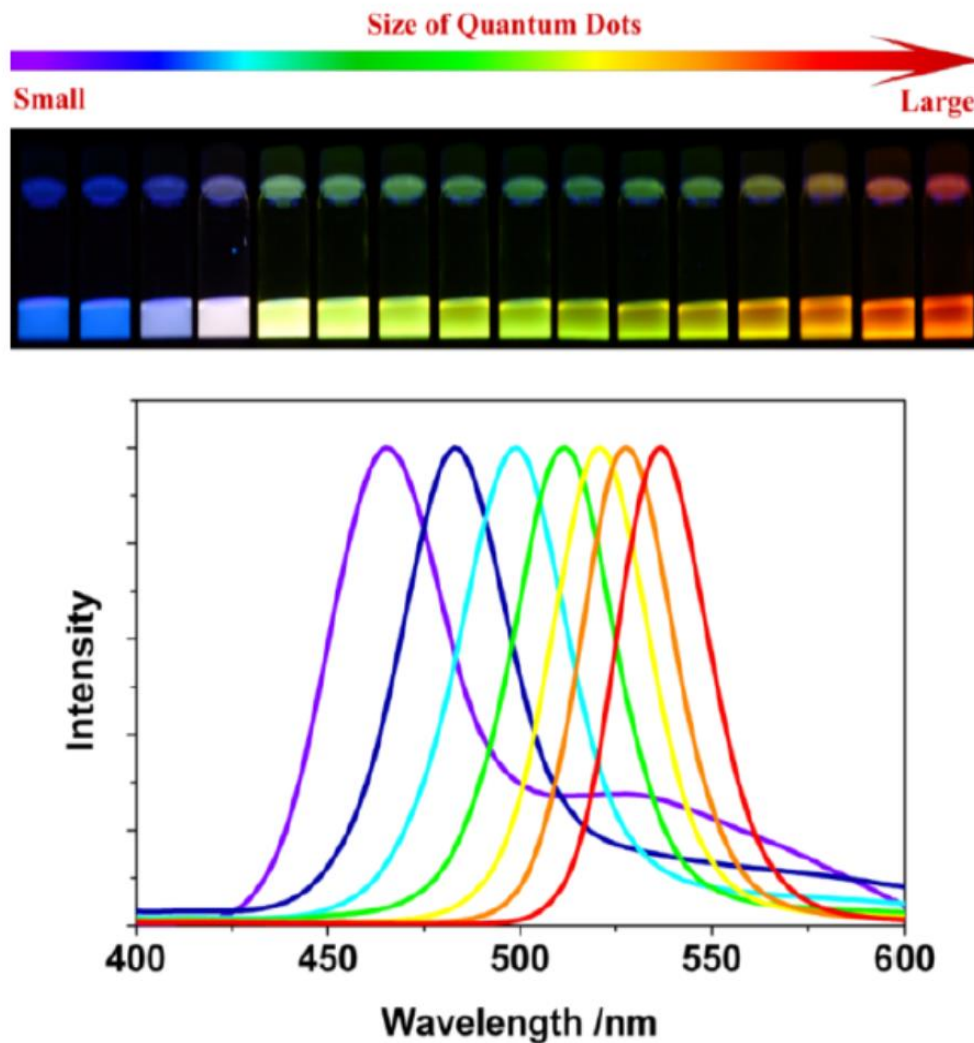
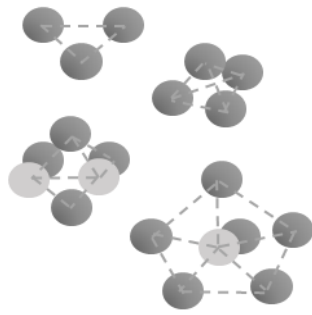
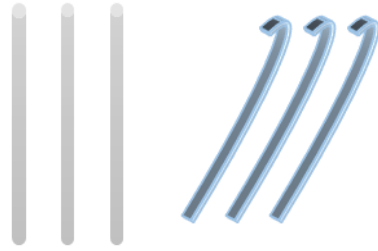


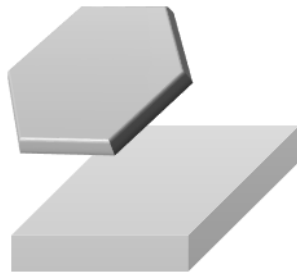
Figure 1.1 Top: Sixteen emission colors from small (blue) to large (red) CdSe Qdots excited by a near-ultraviolet lamp; size of Qdots can be from ~1 nm to ~10 nm. Bottom: Photoluminescence spectra of some of the CdSe Qdots.<sup>8,23)</sup>



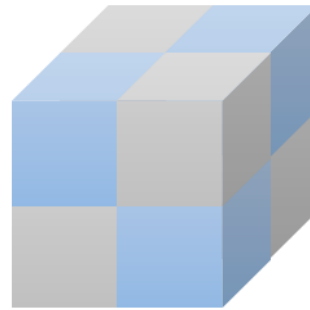
0 D  
structures



1 D  
structures



2 D  
structures



Bulk

**Figure 1.2 Classification of nanostructures based on demensionlity.**

ZnS is one of the most famous II-VI inorganic semiconductors materials with excellent luminescence and physical properties, including a direct wide band gap of 3.77 eV for wurtzite phase and 3.72 eV for cubic phase.<sup>24,25,26</sup> ZnS can adopt three available allotropes: cubic phased zinc blende, hexagonal phased wurtzite, or the rarely observed cubic phased rock salt structures.<sup>27,28</sup> In both zinc blends and wurtzite structures, Zn<sup>2+</sup> and S<sup>2-</sup> ions are tetrahedrally coordinated where only difference is in the stacking sequence of atomic layers.<sup>33</sup> The zinc blende structure and wurtzite structure are shown in Figure 1.4. The stacking sequence along (111) planes within the zinc blende structure exhibits ABCABCABC... pattern, while the stacking sequence along (0001) planes in the wurtzite shows ABABAB... pattern.<sup>33,29,31,30</sup> Zinc blende structure of ZnS is the stable form in the bulk which transforms into wurtzite structures at 1020 °C and melts at 1650 °C.<sup>27</sup> Although wurtzite structure is not stable in bulk ZnS, zinc blende and wurtzite can be transformed from one to another, when a temperature control or an alternate stacking sequence.<sup>30,31,32</sup> Such minor different arrangement of the atoms leads to large difference in properties of these materials.<sup>31</sup>

Due to its excellent properties, many researches has been studying 1D ZnS nanostructures.<sup>33</sup> In 2013, S. M. Jeong et al. have demonstrated the mechanoluminescence from the composite films consisting of ZnS based semiconductor powders and soft polymer matrix of polydimethylsiloxane (PDMS).<sup>34,35,44</sup> many researchers followed to investigate the mechanoluminescence mechanism as well as develop a display utilizing the mechanoluminescence using the copper doped ZnS and manganese doped ZnS.<sup>34,35,36,37</sup>

Mechanoluminescence (ML) is light emission phenomenon resulting from any mechanical deformation of solid. Mechanoluminescence is divided into several categories depending on the mechanical stimulus.<sup>38</sup> For example, mechanoluminescence can be excited by cleaving, scratching, crushing, grinding, and rubbing of crystal surfaces. Francis Bacon was the first to report the emission of light during scrape of sugar crystals in “*Of the Advancement of Learning*”, published in 1605.<sup>39</sup> Another common example of triboluminescence is the emission of blue-green light when a Wint-O-Green Life Saver candy is crushed in the dark.<sup>40</sup> Recently, a variety of mechanoluminescence materials have been developed.<sup>35,36,37,41,42,43</sup> Figure 1.3 shows mechanoluminescence material display produced with the fiber shaped composite of zinc sulfide and polydimethylsiloxane elastomer. These display emit light by the wind. In this thesis, in order to adjust emission wavelength and surface morphology, we synthesized 1D un-doped and transition metal doped ZnS nanostructures using the thermal chemical vapor deposition method, and varied dopant species such as copper and manganese.

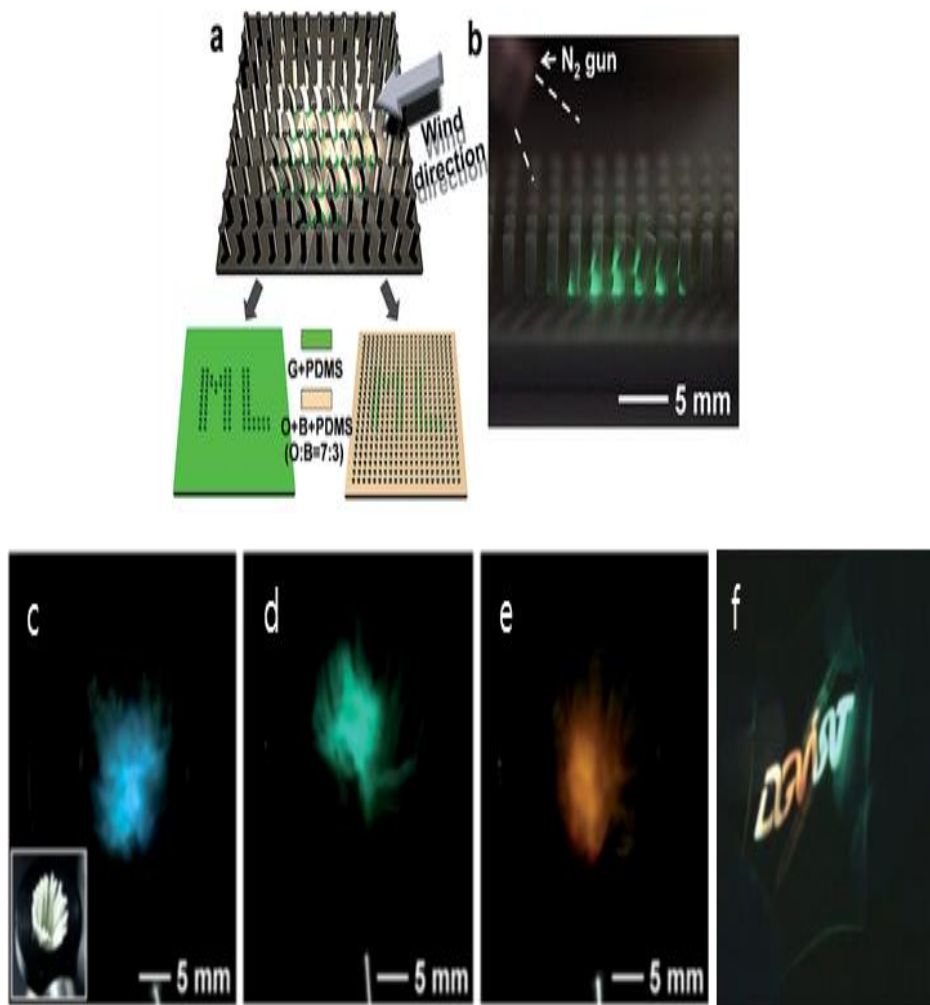


**Figure 1.3 Optical characteristics of the wind-driven ML. (a) Schematic illustration of the set-up. (b) Photograph of the ML image. (c-f) Photographs obtained from wind-driven ML.<sup>44</sup>**

## 1.2 Literature reviews

ZnS is II-VI inorganic semiconductor materials (zinc blend  $E_g \sim 3.72$  eV, wurtzite  $E_g \sim 3.77$  eV) and commercially used as phosphors and electroluminescent devices. In 1994, Bhargava et al. reported for the first time that the photoluminescence of manganese doped ZnS nanocrystals have enhanced quantum luminescence efficiency compared to the bulk.<sup>45</sup> As a consequence, doped ZnS nanocrystals formed a new class of luminescent materials.<sup>46</sup> Since the work of Bhargava et al., Many researchers have studied the luminescence properties of impurity activated ZnS nanocrystals. Zeng et al. produced different morphological Al doped ZnS nano- and micro-scale structures by using thermal evaporation.<sup>47</sup> Borse et al. demonstrated Fe and Ni doped ZnS nanoparticles synthesized by chemical method.<sup>48</sup> As a result, different transition metal ions and rare-earth ions, such as  $\text{Cu}^{2+}$ ,  $\text{Mn}^{2+}$ ,  $\text{Ni}^{2+}$ ,  $\text{Eu}^{3+}$ , ZnS NC's doped with show interesting properties of increased energy band gap compared to that of bulk. Recently, several authors have reported transition metal ion doped ZnS nanocrystals with different technique. Among the different synthesis method, the thermal chemical vapor deposition has attracted a lot of attention due to its distinct advantages in efficient synthesis of 1D nanostructures, adjusted by the temperature, carrier gas flow, and starting materials. In order to examine the characteristics of transition metal doped ZnS nanostructures, we synthesized un-doped and transition metal (Cu, and Mn) doped 1D ZnS nanostructures using the thermal chemical vapor deposition method.

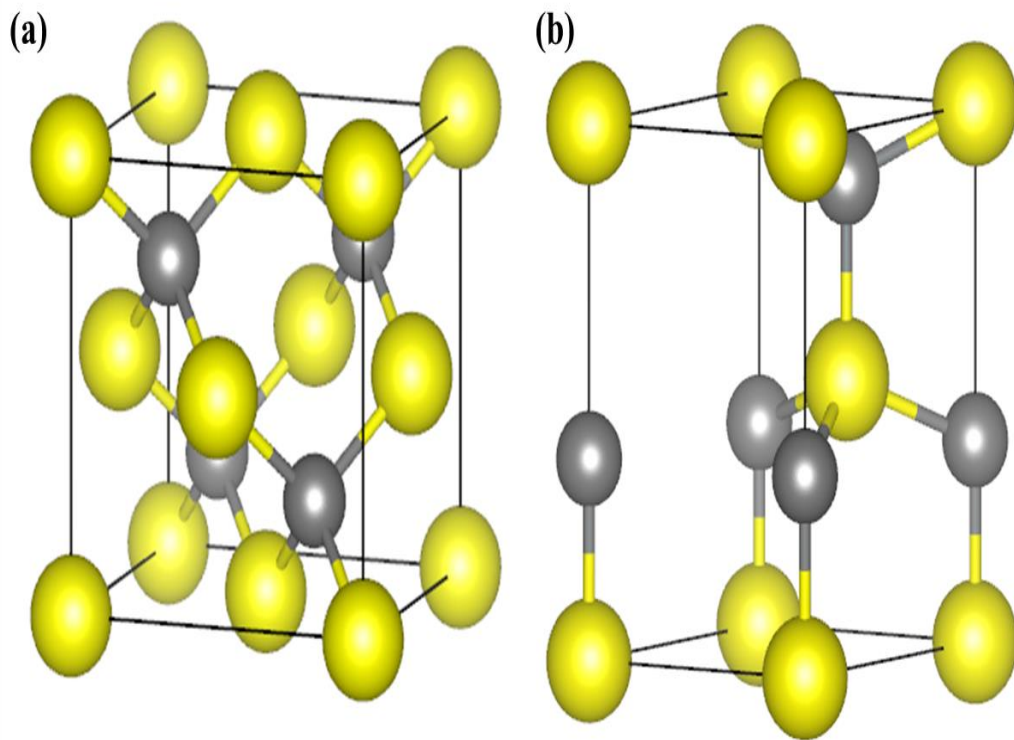


**Figure 1.4 (a) The zinc blende and (b) wurtzite structures. The Yellow represents the sulfur atoms and gray represents the zinc atoms.**

## II. EXPERIMENTAL DETAILS

### 2.1 Synthesis of ZnS nanostructures

There are many methods to synthesize the 1D nanostructures. Among the many methods, chemically synthesis method is the most well-known and widely used. In this section we will briefly reviewed these methods. Figure 2.1 shows the morphologies of ZnS related 1D nanostructures such as nanowire,<sup>16,33</sup> nanobelts,<sup>33, 49</sup> nanotubes,<sup>17</sup> and nanocombs.<sup>50</sup>

#### 2.1.1 Chemical vapor deposition (CVD)

The chemically synthesis method such as thermal chemical vapor deposition (Thermal CVD),<sup>16,19,33,50</sup> metal organic chemical vapor deposition (MOCVD),<sup>33,51</sup> and hydride vapor phase epitaxy (HVPE),<sup>52</sup> is one of the effective method for the synthesis of 1D nanostructures. An important advantage of the Thermal CVD system is that the method can be used to prepare large amount of the desired nanostructures for structurally uniform, simply, effectiveness and reliably.<sup>33</sup> Figure 2.2 shows ZnS nanowire bundles (aligned nanowire) grown on a CdSe substrate that was first deposited on Si (111) using the thermal CVD system, Wang et al. All nanowires are aligned in a direction, and they are uniformly grown along the bundle. Each bundle preserves a single entity maintains a fairly good facet structure.<sup>53</sup> In this thesis, we studied thermal CVD method for making 1D nanostructures and controlled

reaction parameters in order to adjust the morphology during the formation of the nanostructures.

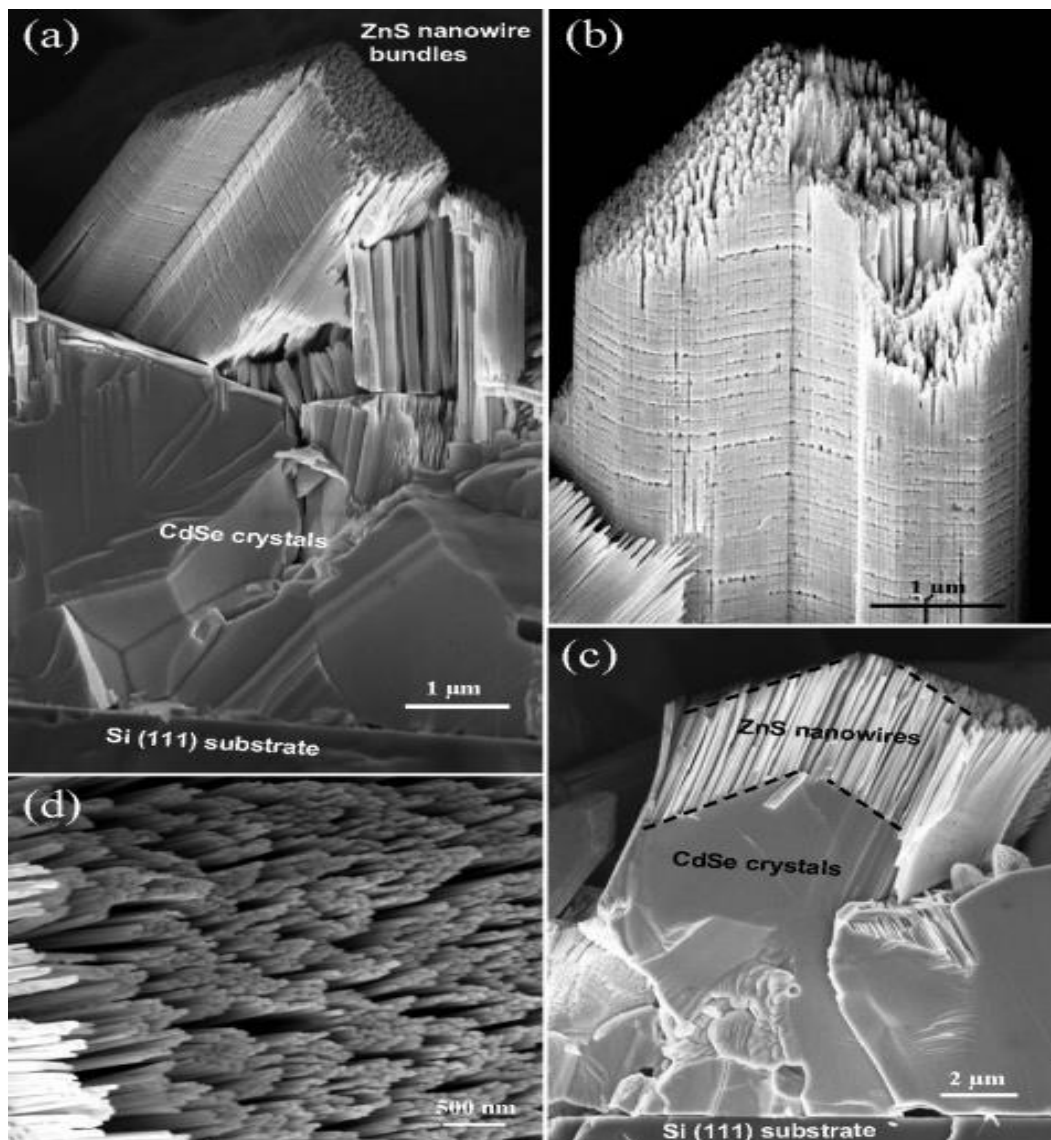


**Figure 2.1 (a) SEM image of ZnS nanowire bundles grown on a CdSe substrate that was first deposited on Si(111). The CdSe is a solid film, but the ZnS is a bundle of aligned nanowires. (b) Enlarged SEM image of a ZnS bundle showing traces created due to fluctuation in growth condition, presenting the equal growth rate of all of the nanowires. (c) Fractured surface of the sample showing the direct growth of ZnS nanowires on the CdSe crystals and the preservation in the ZnS nanowire bundles of the surface morphology of the CdSe crystal. (d) Enlarged top view of the aligned ZnS nanowires.<sup>53</sup>**

## 2.2 Experimental method

### 2.2.1 Experimental materials

Zinc sulfide (ZnS, 99.99%), copper (Cu, 99.9%) and manganese (Mn, 99.9%) powders were purchased from Sigma-Aldrich. gold (Au, 99.99%) sputtering target were purchased from Alfa Aesar. Powder of ZnS, Cu and Mn were used for the starting materials and Au catalytic layer was introduced as promoter for the 1D ZnS nanostructures.

### 2.2.2 Preparation of catalytic layer on substrate

The substrates used in this study were one-side polished n-type single crystal silicon (001) wafer. Silicon (001) wafer was cut into 1cm x 1cm pieces using the dicing saw system (DAD3240, DISCO) and 1cm x 1cm silicon pieces were subjected to sonication cleaning in acetone, methyl alcohol and ethyl alcohol for 10min, respectively. Then, Blow dried with nitrogen gas. Table I shows substrate cleaning procedure and deposit condition. The catalytic layer on substrate were performed by DC magnetron sputtering technique at room temperature. Figure 2.2 shows experimental setup in DC magnetron sputtering system. ~2nm thick gold catalytic layer was deposited on the silicon substrate. Sputtering is a physical vapor deposition technique, in which atoms are ejected from a solid target material is bombarded with energetic ions.<sup>54</sup> This bombardment cause a collisions in the target material's surface. These multiple collisions eject atoms from the surface into the gas phase.

These atoms are then directed towards the target substrate to form a thin film. The number of atoms ejected from the surface per incident ion is called the sputter yield. The ions for the sputtering technique are produced by plasma which is generated above the target material. The atoms sputtered from the surface of the target enter the plasma where they are excited and emit photons.<sup>55</sup> Gold sputtering target were loaded on sputtering gun. cleaned substrate were loaded on a substrate holder and then located at 6.0 cm from the sputtering target to act as deposited substrate for catalytic layer. Sputtering system was pumped down and kept at 4 mTorr, while the high purity argon gas was introduced into the vacuum system to take place plasma. The sputtering target was injected to 30 Watt and kept for 5 seconds. After sputtering was over, the surface of substrate was deposited on gold catalytic layer.

**Table I. Substrate preparation procedure.**

1. Cleaning	i	Sonication in acetone for 10 min
	ii	Sonication in methyl alcohol for 10 min
	iii	Sonication in ethyl alcohol for 10min
	iv	Blow dried with nitrogen gas
2. Deposition		Base pressure : $1.6 \times 10^{-6}$ Torr
		Working pressure : $4 \times 10^{-3}$ Torr
		Power : 30 W
		Target : Gold (Au)
		Gas flow : Ar 20 sccm

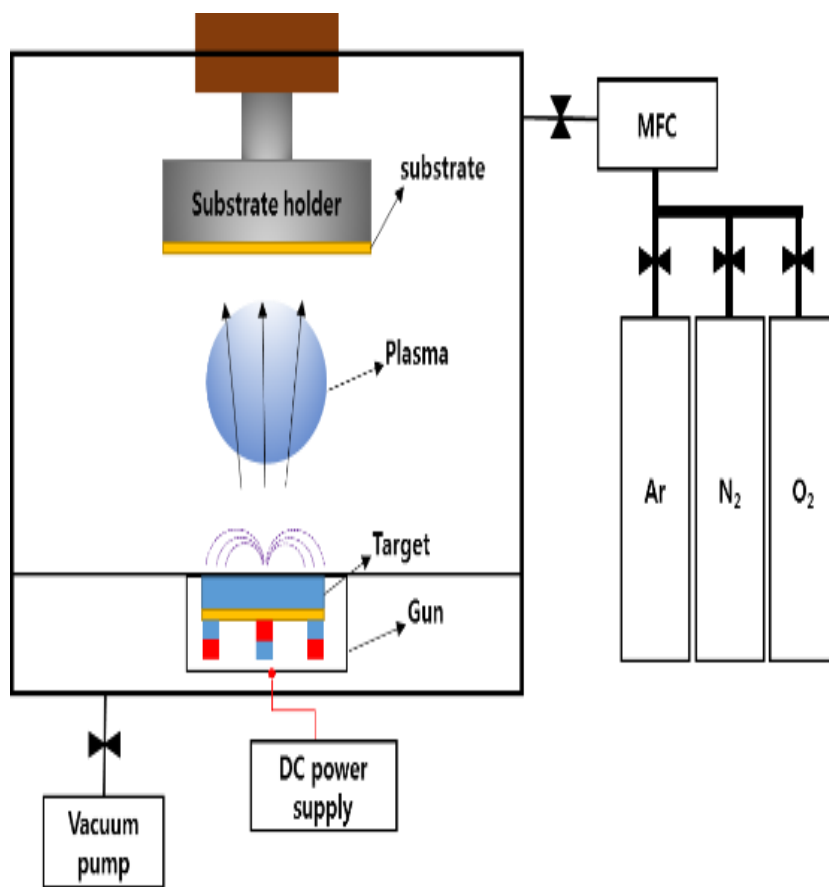


**Figure 2.2 Schematic of the DC magnetron sputtering system.**

### 2.2.3 Synthesis of un-doped / doped ZnS nanostructures

A thermal vapor transport method was used for synthesizing one-dimensional (1D) ZnS nanostructures such as nanorods, nanowire and nanoribbons. The synthesis was performed in a conventional horizontal quartz tube. 1D pure ZnS, Cu doped ZnS, and Mn doped ZnS nanostructures were synthesized on catalytic layer deposited substrates by thermal chemical vapor deposition system (Thermal CVD). Thermal CVD system only uses thermal energy for the activation method, diffusive-convective transport of synthesis process that makes 1D nanostructures at the surface of the growth substrate. In a typical CVD system, the synthesis takes place inside a horizontal quartz tube placed inside a high temperature furnace. Inside the quartz tube, starting material is loaded in a quartz boat and put in the upstream of the tube. In order to effectively synthesize 1D nanostructures, catalytic layer deposited substrate used for collecting the final product is placed downstream. Figure 2.3 (a) shows experimental setup in Thermal CVD system and (b) specific growth procedure. The synthesis parameters were extremely dependent on the source and substrate temperature. (c) Before the synthesis process, heated to 900°C and a movable thermocouple was put into the quartz tube to measure the temperature distribution. Zinc sulfide (50 mg, 99.99%, Sigma-Aldrich) and various doping materials such as copper and manganese were loaded in a quartz boat and then put into the center of quartz tube. Silicon substrate with 2 nm thick gold catalytic layer were located downstream at 15 cm from the center of quartz tube to act as synthesized substrate for 1D ZnS nanostructures. During the synthesis process, Thermal CVD system was pumped down and kept at 10 mTorr, while the high purity argon gas

(99.99%) was introduced into the quartz tube to eliminate the oxide and transport the starting materials. The furnace was dramatically heated to 900 °C at a rate of 50 °C/min and kept for 60 minutes under the 50 sccm argon gas flow. After the synthesis was over, the substrate was cooled naturally. Variety of the synthesis temperature and doping materials were controlled for confirming the influence in the 1D ZnS nanostructures. The specific synthesis parameters are given as tables II and III below.

**Table II. Experimental condition for various temperature.**

	Synthesis temperature	Synthesis time	Pressure	Gas flow	Doping source
ZnS	900 °C				
	1000 °C	60 min	2.54 Torr	Ar 50sccm	None
	1100 °C				

**Table III. Experimental condition for various doping materials.**

	Synthesis temperature	Synthesis time	Pressure	Gas flow	Doping source
ZnS					None
	900 °C	60 min	2.54 Torr	Ar 50sccm	Cu
					Mn

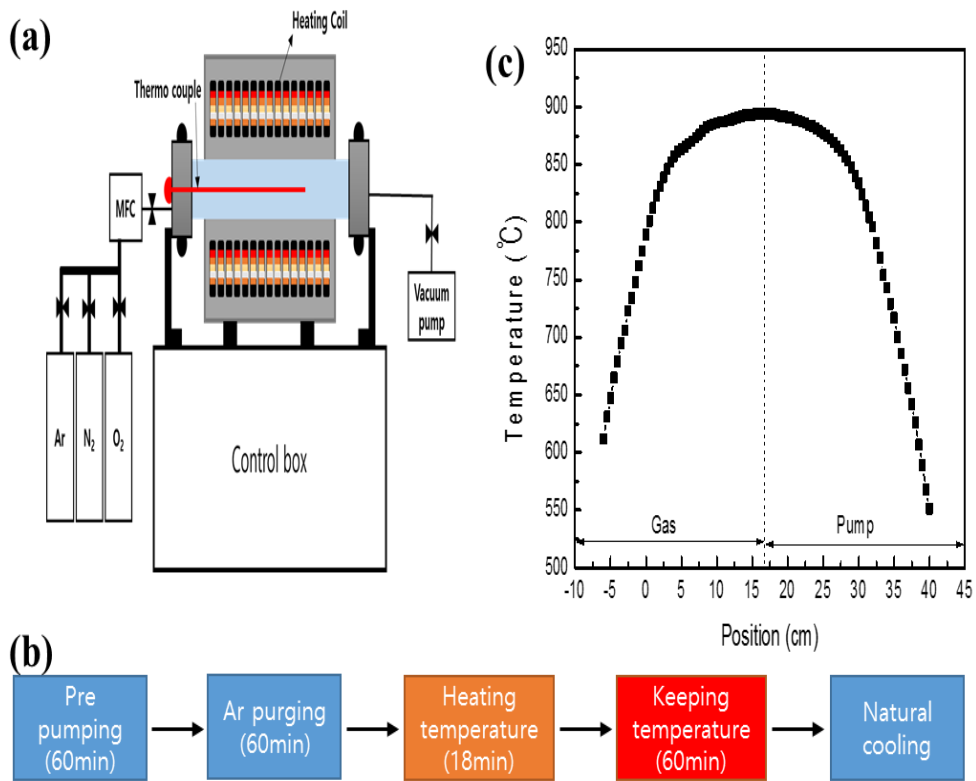


**Figure 2.3 (a) The schematic set up of Thermal CVD system and (b) synthesis process of the 1D ZnS nanostructures with Thermal CVD. (c) Temperature profile of the furnace.**

## 2.3 Characterizations

### 2.3.1 X-ray diffraction (XRD)

X-ray diffraction (XRD) is a one of the most common structural characterizing method for the study of crystal structures and chemical composition of the synthesis products. XRD is based on constructive interference of monochromatic x-rays and crystalline sample. These x-rays are generated by a cathode ray tube, filtered to produce monochromatic radiation, collimated to concentrate, and directed toward the sample. The interaction of the incident x-ray with the sample produces constructive interference when conditions satisfy  $n\lambda=2d\sin\theta$  Bragg's law where n is integer representing the order of the diffraction peak,  $\lambda$  is the wavelength of incident rays, d is inter-planar spacing of the crystal, and  $\theta$  is the diffraction angle (Bragg's angle). Bragg's law relates the wavelength of electromagnetic radiation to the diffraction angle and the lattice parameter in a crystalline sample. Figure 2.4 shows diffraction of x-rays by crystal. By measuring the sample through a range of  $2\theta$  angles, all possible diffraction directions of the lattice should be achieved due to the random orientation of the powdered material. These diffracted x-rays are detected, conversion of the diffraction peaks to d-spacings allows identification of the mineral because each mineral has a set of unique d-spacings. so, this is achieved by comparison of d-spacings with standard reference patterns.<sup>56</sup> In the thesis, 1D ZnS nanostructures were investigated by using Empyrean x-ray diffractometer (PANalytical) equipped with a Empyrean Cu LFF HR x-ray tube (PANalytical) with Cu-K $\alpha$  radiation ( $\lambda=1.54187 \text{ \AA}$ ) from a rotating anode x-ray

generator operating 40kV and 30mA. The XRD optics consisted of soller slits 0.04 rad, mask 10mm, anti-scattering slit 1° and divergence slit 1/2°. HighScore Plus program (PANalytical) used to search XRD pattern and analyze the phases in the samples.

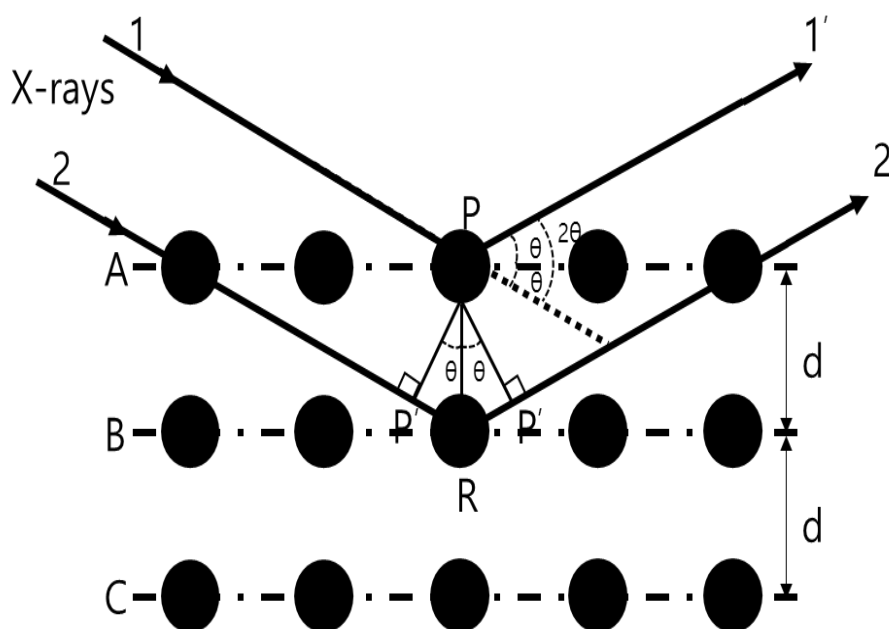


**Figure 2.4 Diffraction of x-rays by a crystal.**

### 2.3.2 Electron microscopy (EM)

The operating principle of the electron microscopy is like a conventional optical microscope (OM). The size of the smallest features that we can distinguish under the optical microscope is on the order of the wavelength of the light. International Commission on Illumination (CIE) established the human eyes have sensitivity to visible light range from 380 nm to 730 nm. This mean that we can't observe smaller than a few hundred nano-scaled sample using visible light system. Electron microscopy work by using an accelerated electron beam instead of visible light. Because electrons beam has the properties of wave with as wavelength that is much smaller than visible light. electron beam allows to measure at nano-scaled sample. It is capable of much higher magnifications and has a greater resolving power than optical microscopy, allowing it to see much smaller objects in finer detail. All electron microscopy uses electromagnetic lenses to control the path of electrons. The basic design of an electromagnetic lens is a solenoid through which one can pass a current, thereby inducing an electromagnetic field. The electron beam passes through the center of such solenoids on its way down the column of the electron microscopy toward the sample. Electron are very sensitive to magnetic field and can therefore be controlled by changing the current through the lenses. Figure 2.5 shows schematic diagram of electron microscope. The resolving power of a microscopy is directly related to the wavelength of the irradiation used to form an image. Reducing wavelength increases resolution. Therefore, the resolution of the microscopy is increased if the accelerating voltage of the electron beam is increased. Also, electron microscopy is equipped with x-ray capabilities, the equipment can generate information

about the elemental of the structures as well as the specific location of those elements. Electron microscopy (EM) is incident into sample by the accelerated electron beam generated by the electron gun. When the accelerated electron beam entrance into the sample, a backscattered electron or secondary electron is emitted. Through these detected signal, we demonstrated surface of the sample and chemical components. Figure 2.6 shows interaction of the electron beam with the sample. Thickness, Size and morphology of the synthesis products were demonstrated by high resolution field emission electron microscopy (HR FE-SEM). The sample was scanned in a HR FE-SEM (SU8020, Hitachi) working at 3kV (or 15kV) accelerating voltage and about 5 mm ~ 8 mm working distance.

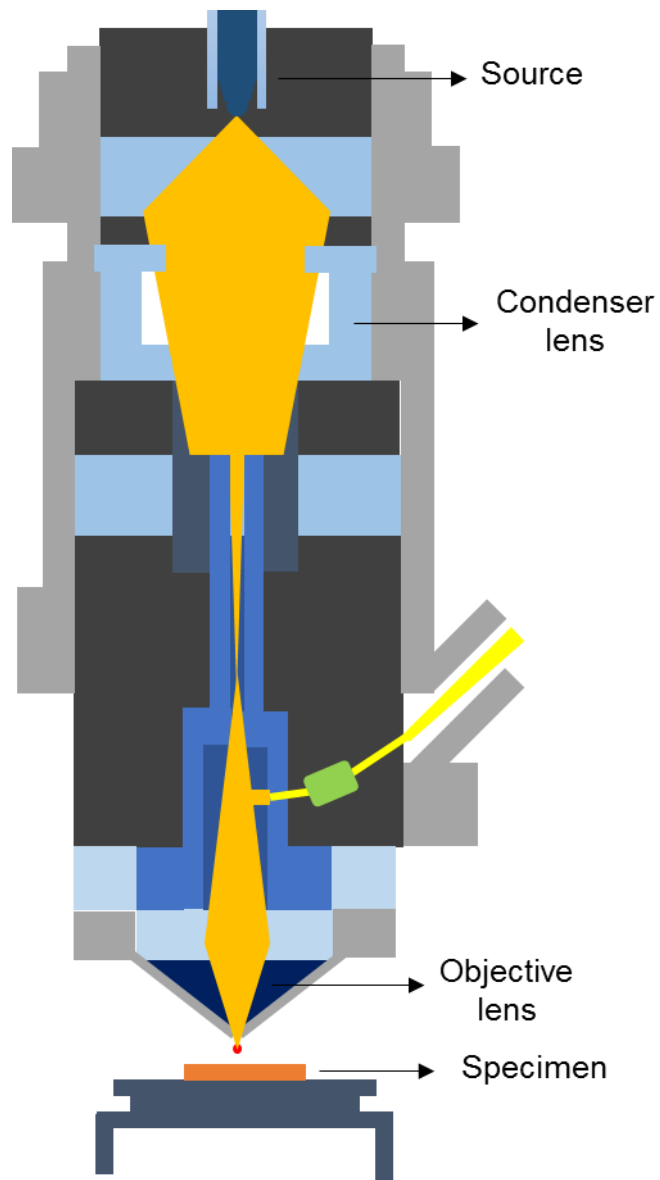


**Figure 2.5 Schematic diagram of scanning electron microscope.**

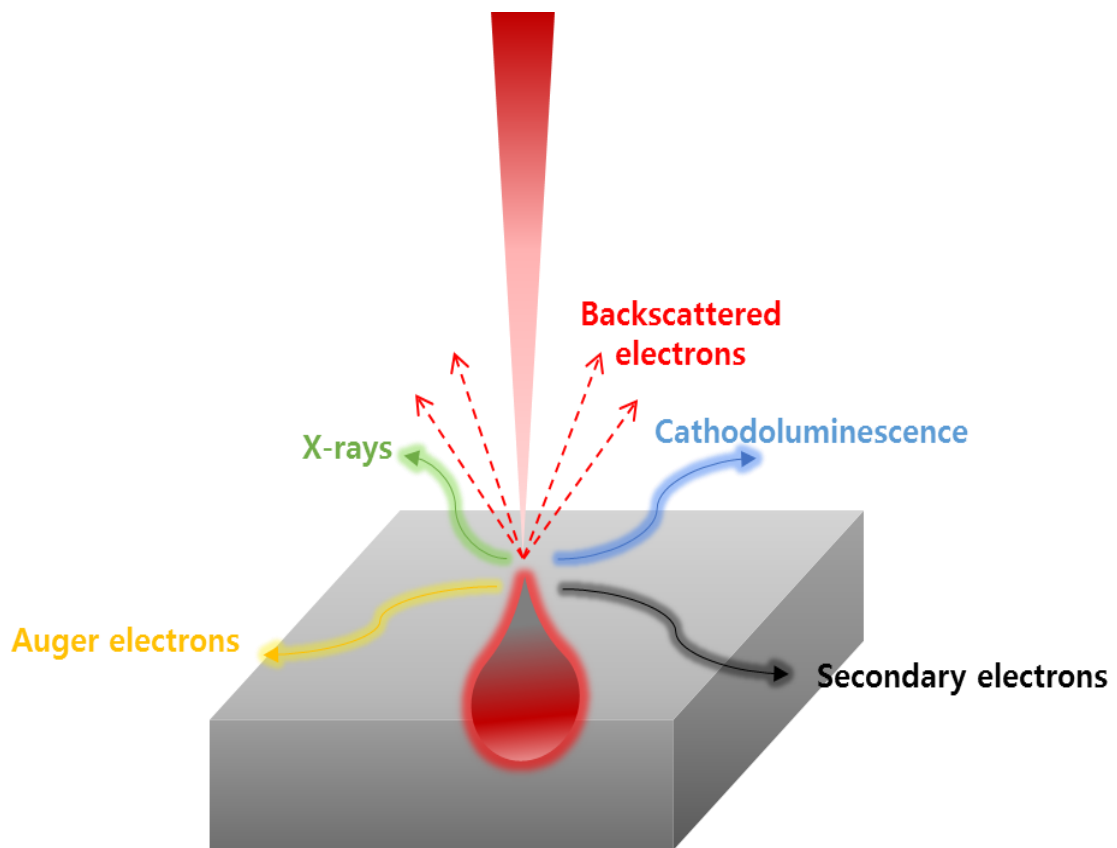


**Figure 2.6 Interaction of the electron beam with the sample; Signal generated when an electron beam is incident on a sample.**

### 2.3.3 Cathodoluminescence (CL)

Cathodoluminescence (CL) is an optical phenomenon in which accelerated high energy electron striking the luminescence material, cause the emission of photons of characteristic wavelengths in the visible spectrum. Cathodoluminescence are used to investigate the distribution of recombination centers in semiconductors including extended defects such as dislocations, grain boundaries, and other important features. Cathodoluminescence has enabled imaging of the electronic and optical properties of semiconductor structures with a spatial resolution of about 50 nm. Also, cathodoluminescence measurement system is equipped with spectroscopy mode. In spectroscopy mode, a spectrum of the emitted light is obtained over a selected area under observation in the electron microscope. Solid-state band theory provides a way to explain the luminescence phenomenon. If a crystal is bombarded by electron with sufficient energy, electrons are excited from the valence band to the conduction band. When the energetic electrons attempt to return to the valence band, electrons may be temporarily trapped by intrinsic (structural defects) or extrinsic (impurities) traps. When the electrons vacate the traps, the energy lost is emitted in the appropriate energy range. Resulting from energy lost, luminescence will occur. In this thesis, cathodoluminescence images and spectra of un-doped and transition metal doped 1D ZnS nanostructures were demonstrated cathodoluminescence measurement system. When an accelerated electron beams are incident on luminescence materials, obtained useful signal including CL. Figure 2.6 shows CL process. The CL measurements in the visible range were demonstrated by panchromatic mode at room

temperature.

### III. RESULT AND DISCUSSION

#### 3.1 Deposit rate of the Au catalytic layer

Catalytic layer on substrate were performed by DC magnetron sputtering technique so as to effectively synthesize 1D nanostructures. thickness of deposited gold thin film, examined by x-ray reflectivity (XRR). We can be estimate that thickness of deposited gold thin film at 30 W, 4 mTorr for 3 min. The thickness of the deposited gold thin film was 47.31 nm for 3 min. Therefore, the deposit rate of gold was  $2.63 \text{ \AA}/\text{sec}$ , ~2nm thick gold catalytic layer were deposited on Si substrate for 7.6 sec.

#### 3.2 Morphology

We have been used the thermal chemical vapor deposition system to synthesize 1D nanostructures. First, in order to confirm the effect of synthesis temperature, synthesized 1D ZnS nanostructures at various temperature with 900, 1000, and 1200 °C. Electron microscopy image of the 1D ZnS structures in Table II and III are presented here in the same order. More details information refer to Table section 2.3.3 and Table II and III of this thesis. Figure 3.2 shows low- and high-magnification EM image of synthesized 1D ZnS

structures at various temperature with (a-b) 900 °C, (c-d) 1000 °C, and (e-f) 1200 °C, respectively. For the scanning electron microscopy measurement, the as-synthesized Si substrate were directly transferred to the scanning electron microscopy chamber without distorting the original nature of the synthesized product. Figure 3.1 (a), (c), and (e) show low magnification EM image of synthesized 1D ZnS structures at various temperature with 900 °C, 1000 °C, and 1200 °C, respectively. Large quantities of ZnS structures were synthesized successfully at various temperatures. Figure 3.1 (a-b) shows a EM image of the synthesis products formed at 900 °C that these products are nanowire. The EM image reveals that randomly orientated nanowires are large scale and have typical diameters of 30 to 60 nm with the lengths up to several ten micrometers. Figure 3.1 (c-d) shows the formation of a randomly orientated ZnS nanostructures that these are nanowire at 1000 °C. The diameter are larger than those of the synthesized nanowire at 900 °C, and the diameter of the nanowires varied within 80 ~ 130 nm. Figure 3.1 (e-f) shows a dramatic change of morphology of synthesized products at 1200 °C. The sub-micro scaled Y-shaped ZnS belts were synthesized at 1200 °C. typical width of 1 ~ 3 μm, a thickness of 300 ~ 500 nm, and lengths of a few millimeters were formed (Figure 3.2 f).

As a result of the above synthesis at various temperatures, 1D ZnS nanostructures were synthesized at 900 °C. Therefore, transition metal doped 1D ZnS nanostructures are performing synthesis at 900 °C. Figure 3.2 shows EM image of transition metal doped 1D ZnS nanostructures synthesized with different dopant species; (a-b) none (c-d) Cu, and (e-f) Mn. Insert is the low magnification EM image of the (a) un-doped (c) Cu

doped and (e) Mn doped ZnS nanostructures, respectively. Large quantities of transition metal doped 1D ZnS nanostructures were synthesized successfully at different dopant species. Figure 3.2 (c-d) shows a EM image of the synthesis products formed with Cu dopant that these products are nanowires. The EM image shows that randomly orientated nanowires have typical diameters of 50 nm. Figure (e-f) shows a substantially change of morphology of synthesized products formed with Mn dopant compared with Cu dopant. Mn doped 1D ZnS structures were formed two different morphologies. The first one is hierarchical urchin-like structures as shown in Figure 3.2 (e). A few micro scaled arrowhead-like structures were formed hierarchical structures. Typically, nanowires with a diameters 50 nm were formed along the tip of the arrowhead-like structures. The other is saw-like structures as shown in Figure 3.2 (f). EM image of a single saw-like structure reveals that the synthesis products consists of numerous 1D saw-like structures have one side with micro-scaled belts and the other side with nano-scaled teeth with a diameters 50 nm. According to the EM image of tooth, part that appear dark in the tooth center. It was supposed that the central tooth consists with other metallic composition or structures.

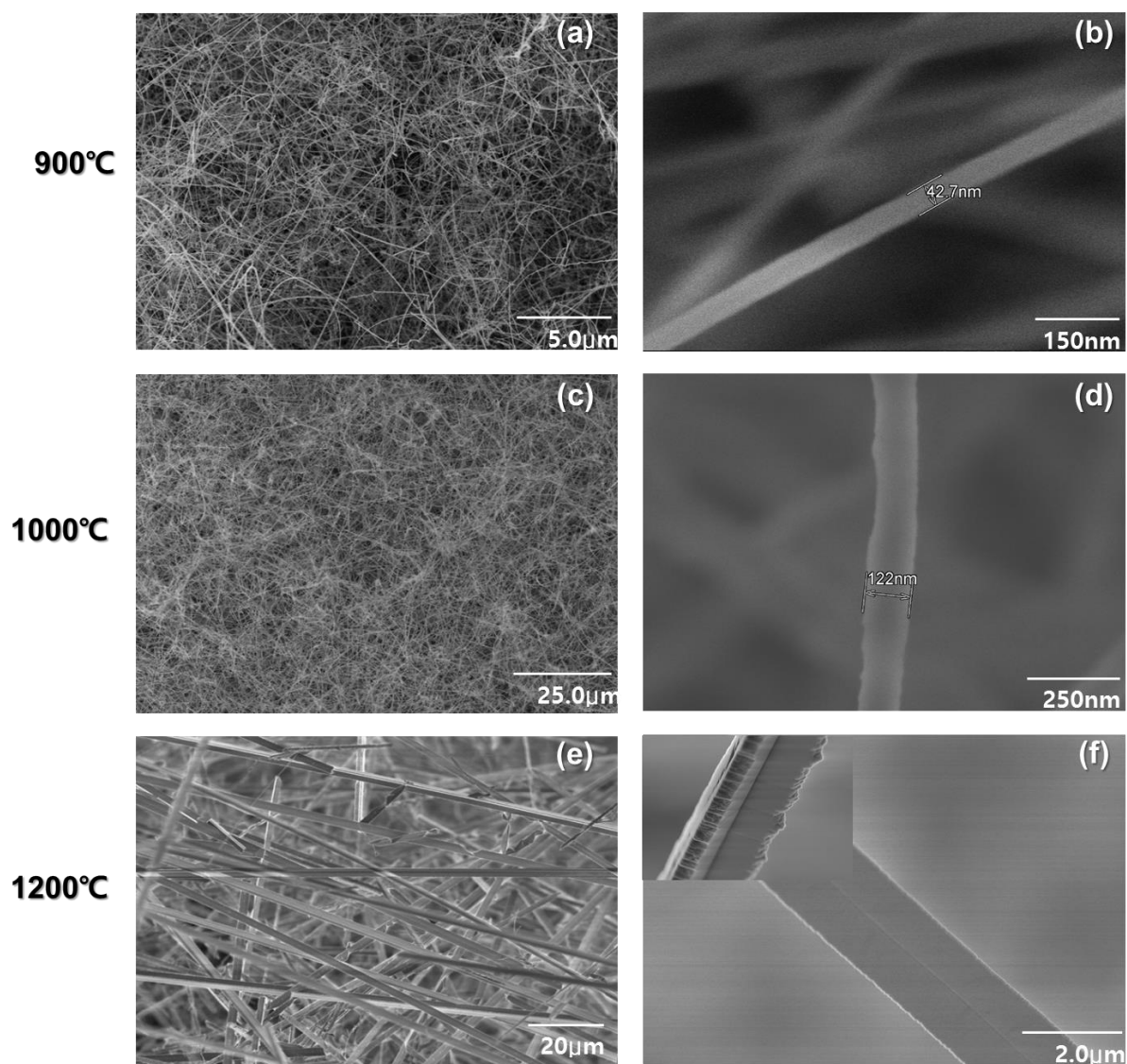


**Figure 3.1 Scanning electron microscopy images showing different morphologies of un-doped 1D ZnS structures synthesized with different set of temperature: (a-b) 900 °C, (c-d) 1000 °C, and (e-f) 1200 °C. Insert is the side-view EM image of the Y-shaped ZnS belts.**

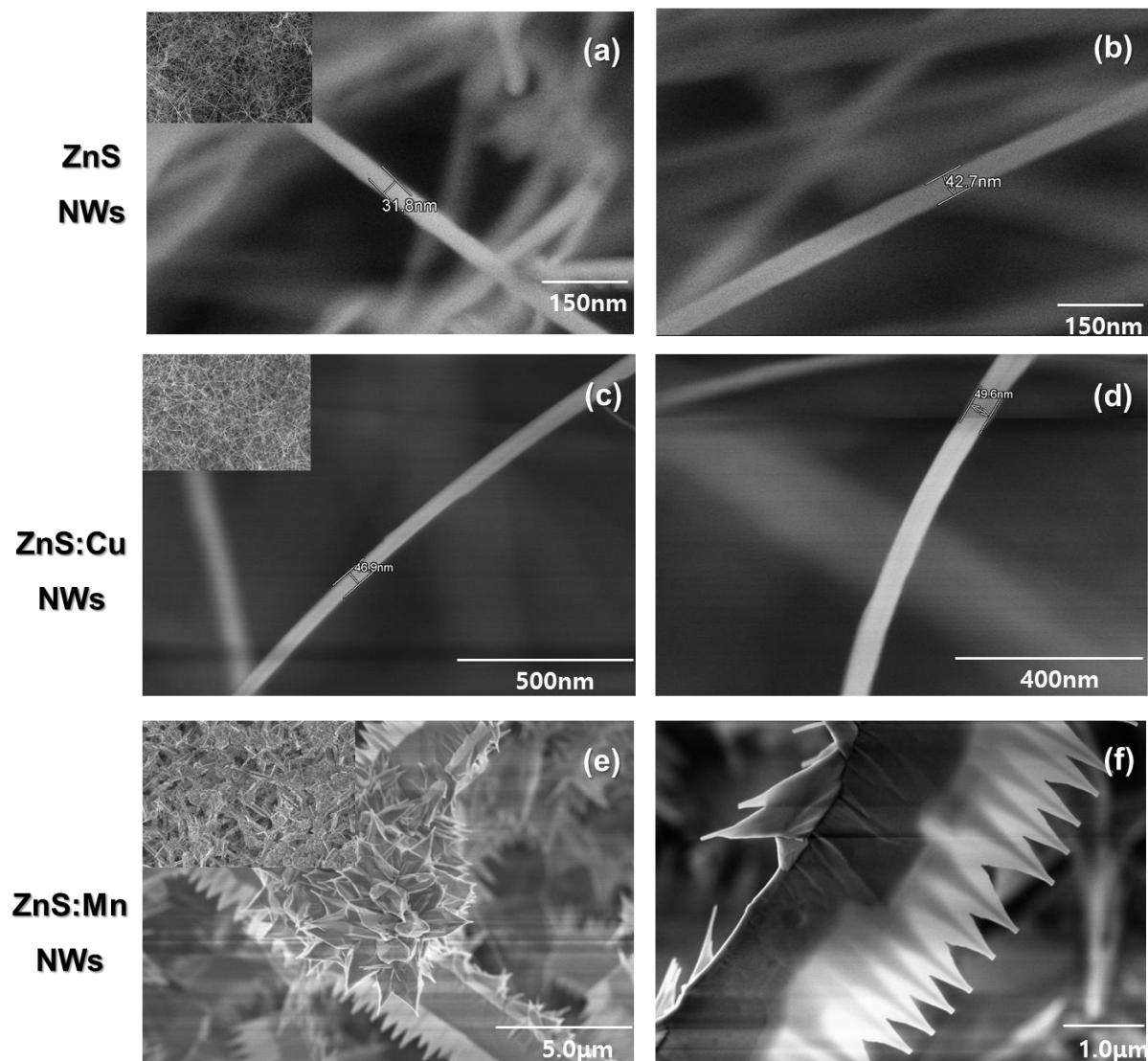


**Figure 3.2 Scanning electron microscopy images showing different morphologies of transition metal doped 1D ZnS nanostructures synthesized with different dopant species (a-b) none, (c-d) Cu, and (e-f) Mn. Insert is the low magnification EM image of the (a) ZnS, (c) ZnS:Cu, and (e) ZnS:Mn NWs respectively.**

### 3.3 Structural properties

Figure 3.3 shows the XRD pattern of synthesis products of un-doped, Cu doped, and Mn doped ZnS nanostructures, respectively. The XRD pattern certainly reveals two kinds of diffraction peaks. In the diffraction pattern, most of the peaks were indexed to the hexagonal phased wurtzite and cubic phased zinc blende ZnS. Those marked with black can be indexed to hexagonal phased wurtzite ZnS (ICSD file: 98-004-3597). The others marked with red can be indexed to cubic phased zinc blende ZnS (ICSD file: 98-065-1457). With the diffraction peaks in the XRD pattern, the synthesized products were concluded as the mixed phase of hexagonal phased wurtzite structure and cubic phased zinc blende structure. Furthermore, hexagonal phased wurtzite structure and cubic phased zinc blende structures exhibits a space group of P-63 mc and F-43 m respectively. The peaks at  $2\theta = 26.96, 30.57, 39.66, 51.83, 55.53, 56.44, 57.65, \text{ and } 72.95^\circ$  correspond to the (010), (011), (012), (013), (020), (021), (022), and (023) planes of hexagonal phased wurtzite ZnS.  $2\theta = 28.59, 33.16, 47.59, 59.19, \text{ and } 69.58^\circ$  agrees well with the (111), (002), (022), (222), and (004) planes of the cubic phased zinc blende ZnS. Because the (112) planes of the hexagonal phased wurtzite ZnS overlap with the (113) planes of the cubic phased zinc blende ZnS. Revealing that the doping of Cu and Mn does not change the crystal structures. In all patterns, Mn or Cu corresponding to impurities were not found. un-, Cu, and Mn doped ZnS nanostructures can be regarded as a mixture of wurtzite and zinc blende structures with a dominant zinc blende ZnS except for Mn doped ZnS nanostructure.

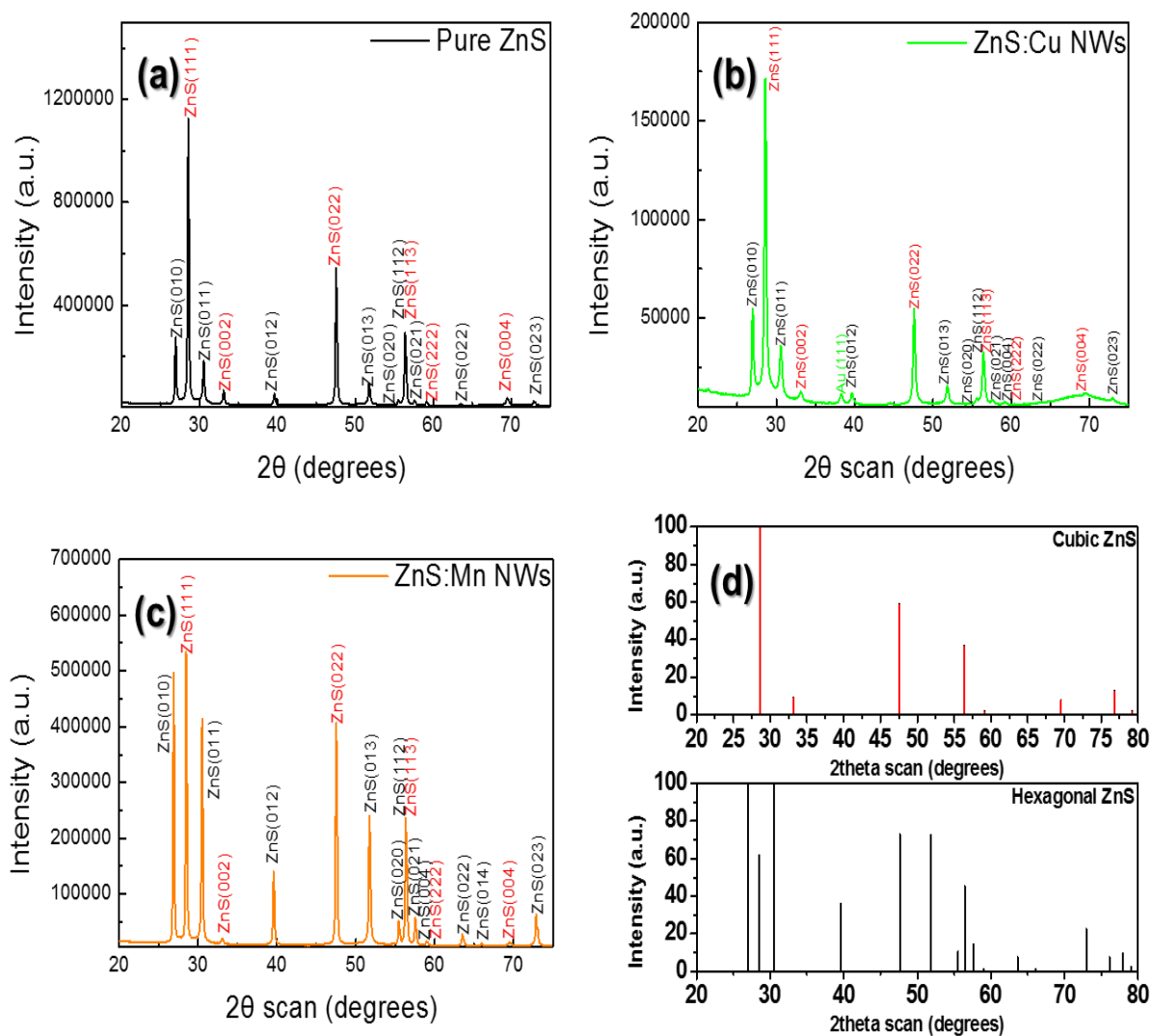


**Figure 3.3** XRD pattern of synthesized products of (a) un-doped, (b) Cu doped, and (c) Mn doped ZnS nanostructures. And XRD pattern of ICSD reference files of cubic and hexagonal phased ZnS.

### 3.4 Luminescence properties

It was confirmed that un-doped, Cu, and Mn doped ZnS nanostructures showed different morphologies. Comparing the CL emission from un-doped, Cu, and Mn doped ZnS nanostructures, confirmed the emission wavelength. Figure 3.4 (a) shows the CL spectrum at

room temperature of un-doped 1D ZnS nanostructures, and the peak revealed a strong green emission at 516 nm (2.40 eV). According to a previous research result on ZnS nanostructures, the strong green emission at 516 nm is related to Au impurity deep levels in the bandgap. In our experiment, Au thin film (~2 nm) is introduced as catalyst. Au thin film (~2 nm) was reacted with ZnS vapor to Au – Zn - S alloy. When Au ions are incorporated in ZnS host lattice, the luminescence centers of Au ions are formed. Therefore, the luminescence peak at long wavelength (516 nm) may result from the trapped electrons and holes states of the Au ion incorporated into ZnS host lattice .<sup>57</sup>

Figure 3.4 (b) shows the CL spectrum at room temperature of Cu doped 1D ZnS nanostructures, composed of three peaks at 430, 460, and 496 nm. The blue emission at 430 nm (2.88 eV) is assigned to the sulfur vacancies states, transition from the trapped electron on sulfur vacancies to interstitial sulfur state produces the blue emission.<sup>58</sup> The emission peak at 460 nm (2.69 eV) is attributed to the transition from the conduction band of ZnS to the  $t_2$  state of the  $\text{Cu}^{2+}$  ions, produces the blue emission band,<sup>59</sup> and the emission peak at 496 nm (2.5eV) arises from the transition between the sulfur vacancies (donor level) state and  $t_2$  state of  $\text{Cu}^{2+}$  ion.<sup>60</sup> Hence from the CL spectrum at room temperature of Cu doped 1D ZnS nanostructures, it can be concluded that Cu ions are incorporated successfully into the ZnS host lattice.

Figure 3.4 (c) shows the CL spectrum at room temperature of Mn doped 1D ZnS nanostructures, and the peak revealed the wavelength at 332, 430, 516, and 582 nm. The wavelength at 332 nm (3.73eV) is closed to the bandgap of bulk ZnS. The blue (430 nm)

emission exhibited for the Au impurity level in ZnS lattice.<sup>57,58,61</sup> The green (516 nm) is attributed to the transition from the sulfur vacancies to zinc vacancies state.<sup>61,62,63,64</sup> Whereas the orange emission at 582 nm (2.13 eV) is associated with Mn dopant, transition from the  $^4T_1(G)$  to  $^6T_1(S)$  state of  $Mn^{2+}$  ion in ZnS host lattice.<sup>58</sup>

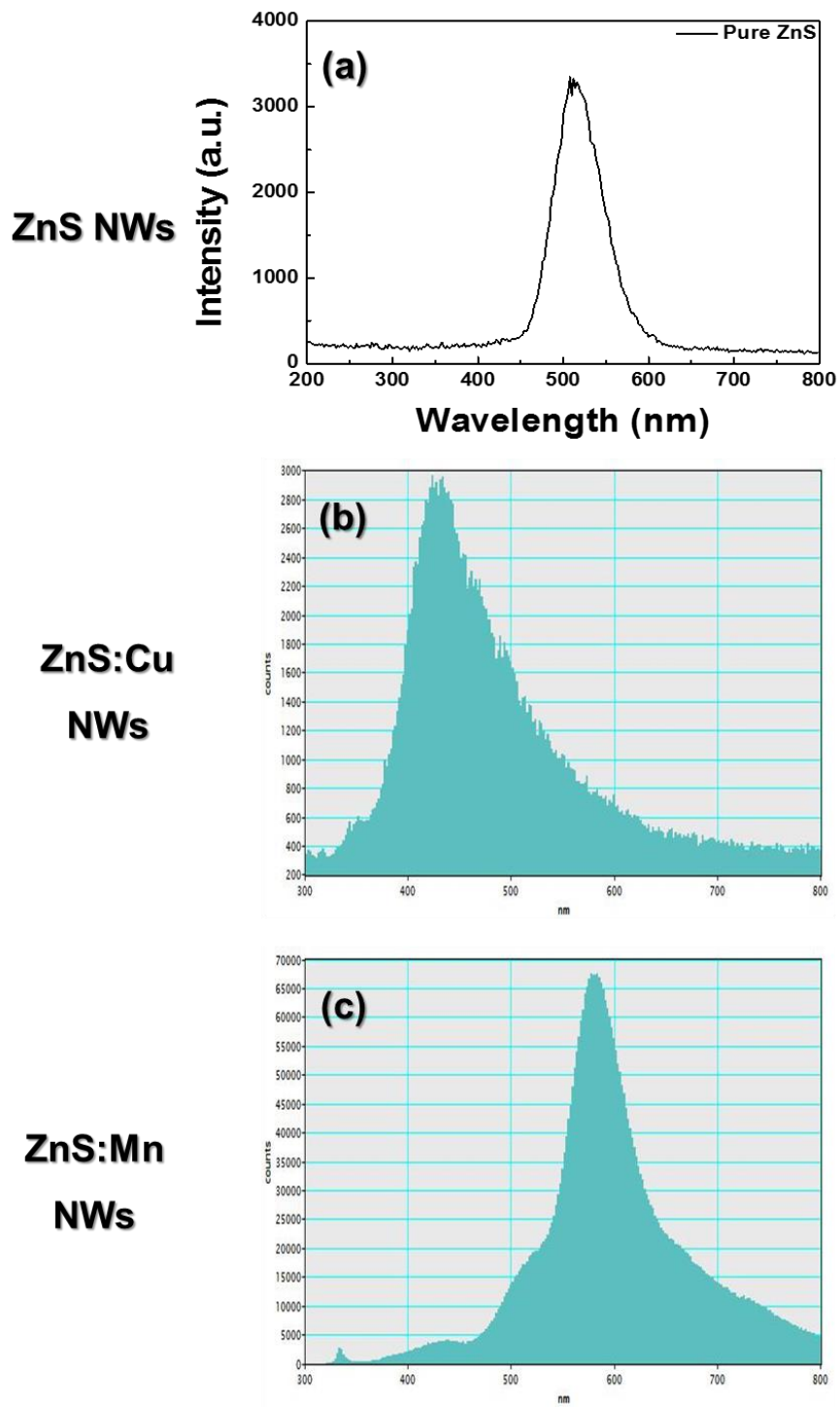


**Figure 3.4** Room temperature CL Spectra of (a) un-doped, (b) Cu, and (c) Mn doped 1D ZnS nanostructures.

## IV. CONCLUSIONS

In conclusion, we successfully synthesized un-doped, Cu doped, and Mn doped ZnS nanostructures by using a chemical vapor deposition method at 900 °C. Electron microscopy confirms that the un-doped and Cu doped ZnS nanostructures are randomly orientated nanowire, typical diameters 30 to 60 nm with the lengths up to several ten micrometers. While the Mn doped ZnS nanostructures were sub-micro scaled hierarchical urchin-like and arrowhead-like structures. The XRD confirmed that the un-doped, Cu doped, and Mn doped ZnS nanostructures were concluded as the mixed phase of hexagonal phased wurtzite and cubic phased zinc blende structure. Comparing the CL spectrum at room temperature of un-doped, Cu doped, and Mn doped ZnS nanostructures, various visible emission properties were investigated. CL spectrum of Cu doped ZnS nanostructures composed of three peaks at 430, 460, and 496 nm, is attributed to the transition from the sulfur vacancies to interstitial sulfur state, conduction band of ZnS to the  $t_2$  state of the  $\text{Cu}^{2+}$  ion, and sulfur vacancies to  $t_2$  state of  $\text{Cu}^{2+}$  ion, respectively. CL spectrum of Mn doped ZnS nanostructures composed of fourth peak at 332, 430, 516, and 582 nm, is attributed to the transition from the conduction to valence band, sulfur vacancies to interstitial sulfur state, sulfur vacancies to zinc vacancies state, and  ${}^4T_1(G)$  to  ${}^6T_1(S)$  state of  $\text{Mn}^{2+}$  ion in ZnS host lattice. In this work, using the transition metal species, various visible emission characteristics were demonstrated in un-doped, Cu doped, and Mn doped ZnS nanostructures and may help to design and control defect states to tune the ZnS properties for the application

in light emitting diodes, and optical sensors.

## Reference

- <sup>1</sup> G. Zhang, K. Tateno, H. Gotoh, and T. Sogawa, *Towards New Low-dimensional Semiconductor Nanostructures and New Possibilities*. NTT Technical Review, 2010, **8**, 1-8.
- <sup>2</sup> C. Buzea, I. I. Pacheco, and K. Robbie, *Nanomaterials and nanoparticles: Sources and toxicity*. *Biointerphases*, 2007, **2**, MR17-71.
- <sup>3</sup> K. Narendra, K. Sunita, *Essentials in Nanoscience and Nanotechnology*. Wiley, 2016.
- <sup>4</sup> M. A. Kastner, *Artificial Atoms*. *Phys. Today*, 1993, **46**, 24-31.
- <sup>5</sup> M. A. Reed, *Quantum Dots*. *Sci. Am.*, 1993, **268**, 118-123.
- <sup>6</sup> R. Turton, *The Quantum Dot: A Journey into the Future of Microelectronics*. Oxford Univ. Pr., 1995.
- <sup>7</sup> P. D. Yang, Y. Y. Wu, and R. Fan, *INORGANIC SEMICONDUCTOR NANOWIRES*. *Int. J. Nanosci.*, 2002, **1**, 1-39.
- <sup>8</sup> C. B. Murray, D. J. Norries, and M. G. Bawendi, *Synthesis and characterization of nearly monodisperse CdE (E = sulfur, selenium, tellurium) semiconductor nanocrystallites*. *J. Am. Chem. Soc.*, 1993, **115**, 8706-8715.
- <sup>9</sup> P. Buffat, and J. P. Borel, *Size effect on melting temperature of gold particles*. *Phys. Rev. A*, 1976, **13**, 2287-2298.
- <sup>10</sup> S. M. Kang, S. S. Ha, W. G. Jung, M. S. Park, H. S. Song, B. J. Kim, and J. I. Hong, *Two-dimensional nanoplates of Bi<sub>2</sub>Se<sub>3</sub> and Bi<sub>2</sub>Te<sub>3</sub> with reduced thermal stability*. *AIP Adv.*, 2016, **6**, 025110.

- <sup>11</sup> J. I. Hong, J.I. Choi, S. S. Jang, J. Y. Gu, Y. L. Chang, G. Wortman, R. L. Snyder, and Z. L. Wang, *Magnetism in Dopant-Free ZnO Nanoplates*. *Nano Lett.* 2012, **12**, 576-581.
- <sup>12</sup> J. Liu, J. F. Ma, Y. Liu, Z. W. Song, Y. Sung, J. R. Fang, and Z. S. Liu, *Synthesis of ZnS nanoparticles via hydrothermal process assisted by microemulsion technique*. *J. Alloys Compd.*, 2009, **486**, L40-L43.
- <sup>13</sup> G. P. Li, J. F. Zhai, D. Li, X. O. Fang, H. Jiang, Q. Z. Dong, and E. K. Wang, *One-pot synthesis of monodispersed ZnS nanospheres with high antibacterial activity*. *J. Mater. Chem.*, 2010, **20**, 9215-9219.
- <sup>14</sup> C. X. Li, D. Y. Jiang, L. L. Zhang, L. F. Xia, and Q. Li, *Controlled Synthesis of ZnS Quantum Dots and ZnS Quantum Flakes with Graphene as a Template*. *Langmuir*, 2012, **28**, 9729-9734.
- <sup>15</sup> X. J. Xu, L. F. Hu, N. Gao, S. X. Liu, S. W. A. Ahmed, A. Ghamdi, A. Alshahrie, and X. S. Fang, *Controlled Growth from ZnS Nanoparticles to ZnS-CdS Nanoparticles Hybrids with Enhanced Photoactivity*. *Adv. Funct. Mater.*, 2015, **25**, 445-454.
- <sup>16</sup> Z. X. Zhang, H. J. Yuan, D. F. Liu, L. F. Liu, J. Shen, Y. J. Xiang, W. J. Ma, W. Y. Zhou, and S. S. Xie, *Growth of ultrafine ZnS nanowires*. *Nanotechnology*, 2007, **18**, 145607-145611.
- <sup>17</sup> X. P. Shen, M. Han, J. M. Hong, Z. L. Xue, and Z. Xu, *Template-Based CVD Synthesis of ZnS Nanotube Arrays*. *Chem. Vap. Deposition*, 2005, **11**, 250-253.
- <sup>18</sup> M. S. Arani, and M. S. Niasari, *Synthesis and characterization of wurtzite ZnS nanoplates through simple solvothermal method with a novel approach*. *J. Ind. Eng. Chem.*, 2014,

**20**, 3179-3185.

- <sup>19</sup> D. S. Li, *Fast and mass synthesis of ZnS nanosheets via an ultra-strong surface interaction*. Cryst. Eng. Comm., 2013, **15**, 10631-10637.
- <sup>20</sup> W. Tong, T. K. Tran, W. Park, S. Schon, B. K. Wagner, and C. J. Summers, *High-quality ZnS thin-film growth for flat-panel displays*. J. Soc. Inf. Disp., 2012, **18**, 325-329.
- <sup>21</sup> H. Dehghani, S. Khoramnejadian, M. Mahboubi, M. Sasani, S. Ghobadzadeh, S. M. Haghghi, and M. Negahdary. *Bilirubin Biosensing by Using of Catalase and ZnS Nanoparticles as Modifier*. Int. J. Electrochem. Sci., 2016, **11**, 2029-2045.
- <sup>22</sup> Y. C. Chen, C. Y. Huang, H. C. Yu, and Y. K. Su. *Nonvolatile memory thin film transistors using CdSe/ZnS quantum dot-poly(methyl methacrylate) composite layer formed by a two-step spin coating technique*. J. Appl. Phys., 2012, **112**, 034518.
- <sup>23</sup> D. Bera, L. Qian, P. H. Holloway, *Semiconducting Quantum Dots for Bioimaging*. InformaHeathcare: New York, NY, USA, 2009, **191**.
- <sup>24</sup> D. Moore, and Z. L. Wang, *Growth of anisotropic one-dimensional ZnS nanostructures*. J. Mater. Chem., 2006, **16**, 3898-3905.
- <sup>25</sup> X. S. Fang, Y. Bando, U. K. Gautam, C. H. Ye, and D. Golberg, *Inorganic semiconductor nanostructures and their field-emission applications*. J. Mater. Chem., 2008, **18**, 509-522.
- <sup>26</sup> J. Yan, X. S. Fang, L. Zhng, Y. Bando, U. K. Gautam, B. Dierre, T. Sekiguchi, and D. Golberg, *Structure and Cathodoluminescence of Individual ZnS/ZnO Biaxial Nanobelt Heterostructures*. Nano Lett., 2008, **8**, 2794-2799.

- <sup>27</sup> F. A. L. Porta, L. Gracia, J. Andres, J. R. Sambrano, J. A. Varela, and E. Longo, *A DFT Study of Structural and Electronic Properties of ZnS Polymorphs and its Pressure-Induced Phase Transitions*. J. Am. Ceram. Soc., 2014, **97**, 4011-4018.
- <sup>28</sup> F. A. L. Porta, J. Andres, M. S. Li, J. R. Sambrano, J. A. Varela, and E. Longo, *Zinc blende versus wurtzite ZnS nanoparticles: control of the phase and optical properties by tetrabutylammonium hydroxide*. Phys. Chem. Phys., 2014, **16**, 20127-20137.
- <sup>29</sup> H. Zheng, J. Wang, J. Y. Huang, J. B. Wang, Z. Zhang, and S. X. Mao, *Dynamic Process of Phase Transition from Wurtzite to Zinc Blende Structure in InAs Nanowires*. Nano Lett., 2013, **13**, 6023-6027.
- <sup>30</sup> Y. Dong, X. D. Wang, and Z. L. Wang, *Phase controlled synthesis of ZnS nanoblets: zinc blende vs wurtzite*. Chem. Phys. Lett., 2004, **398**, 32-36.
- <sup>31</sup> C. Y. Yeh, Z. W. Lu, S. Froyen, and A. Zunger, *Zinc-blende-wurtzite polytypism in semiconductors*. Phys. Rev. B, 1992, **46**, 10086-10097.
- <sup>32</sup> S. B. Qadri, E. F. Skelton, D. Hsu, A. D. Dinsmore, J. Yang, H. F. Gray, and B. R. Ratna, *Size-induced transition-temperature reduction in nanoparticles of ZnS*. Phys. Rev. B, 1999, **60**, 9191-9193.
- <sup>33</sup> X. S. Fang, Y. Bando, M. Y. Liao, U. K. Gautam, C. Y. Zhi, B. Dierre, B. D. Liu, T. Y. Zhai, T. Sekiguchi, Y. Koide, and D. Golberg, *ZnS nanostructures: From synthesis to applications*. Prog. Mater. Sci., 2011, **56**, 175-287.
- <sup>34</sup> S. M. Jeong, S. K. Song, S. K. Lee, and B. D. Choi, *Mechanically driven light-generator with high durability*. Appl. Phys. Lett., 2013, **101**, 051110.

- <sup>35</sup> S. M. Jeong, S. K. Song, S. K. Lee, and N. Y. Ha, *Color Manipulation of Mechanoluminescence from Stress-Activated Composite Films*. *Adv. Mater.*, 2013, **25**, 6194-6200.
- <sup>36</sup> R. Sharama, D. P. Bisen, S. J. Dhoble, N. Brahme, and B. P. Chandra, *Mechanoluminescence and thermoluminescence of Mn doped ZnS nanocrystals*. *J. Lumin.*, 2011, **131**, 2089-2092.
- <sup>37</sup> V. K. Chandra, B. P. Chandra, and J. Piyush, *Self-recovery of mechanoluminescence in ZnS:Cu and ZnS:Mn phosphors by trapping of drifting charge carriers*. *Appl. Phys. Lett.*, 2013, **103**, 161113.
- <sup>38</sup> P. B. O'Hara, C. Engelson, and W. St. Peter, *Turning on the Light: Lessons from Luminescence*. *J. Chem. Edu.*, 2005, **82**, 49-52.
- <sup>39</sup> F. Bacon, *Of the Advancement of Learning*. 1605, G. W. Kitchin, Ed., London: J. M. Dent and Sons, 1951. (Original work published in 1605)
- <sup>40</sup> B. P. Chandra, and D. R. Vij, *Luminescence of Solids*. Plenum, New York., 1988, 361-389.
- <sup>41</sup> D. P. Bisen, and R. Sharma, *Mechanoluminescence properties of SrAl<sub>2</sub>O<sub>4</sub>: Eu<sup>2+</sup> phosphor by combustion synthesis*. *Luminescence*, 2016, **31**, 394-400.
- <sup>42</sup> T. Dong, C. N. Xu, Y. Fujio, and A. Yoshida, *Mechanism of mechanical quenching and mechanoluminescence in phosphorescent CaZnOS:Cu*. *Light, Sci. Appl.*, 2015, **4**, e356-e359.
- <sup>43</sup> W. B. Mcnamara III, Y. T. Didenko, and K. S. Suslick, *Sonoluminescence temperatures during multi-bubble cavitation*, *NATURE*, 1999, **401**, 772-775.

- <sup>44</sup> S. M. Jeong, S. K. Song, K. I. Joo, J. W. Kim, S. H. Hwang, J. W. Jeong, and H. M. Kim, *Bright, wind-driven white mechanoluminescence from zinc sulphide microparticles embedded in a polydimethylsiloxane elastomer*. Energy Environ. Sci., 2014, **7**, 3338-3346.
- <sup>45</sup> R. N. Bhargava, D. Gallagher, X. Hong, and A. Nurmikko, *Optical Properties of Manganese-Doped Nanocrystals of ZnS*. Phys. Rev. Lett., 1994, **72**, 416-419.
- <sup>46</sup> R. N. Bhargava, D. Gallagher, and T. Welker, *Doped nanocrystals of semiconductors – a new class of luminescent materials*. J. Lumin, 1994, **60&61**, 275-280.
- <sup>47</sup> X. H. Zeng, S. J. Yan, J. Y. Cui, H. F. Liu, J. Dong, W. W. Xia, M. Zhou, and H. Chen, *Size- and morphology-dependent optical properties of ZnS:Al one-dimensional structures*. J. Nanopart. Res., 2015,**17**, 187.
- <sup>48</sup> P. H. Borse, N. Deshmukh, R. F. Shinde, S. K. Date, and S. K. Kulkarni, *Luminescence quenching in ZnS nanoparticles due to Fe and Ni doping*. J. Mat. Sci., 1999, **34**, 6087-6093.
- <sup>49</sup> B. D. Liu, B. Yang, B. Dierre, T. Sekiguchi, and X. Jiang, *Local defect-induced red-shift of cathodoluminescence in individual ZnS nanobelts*. Nanoscale. Nanoscale, 2014, **6**, 12414-12420.
- <sup>50</sup> C. Y. Lan, J. F. Gong, Y. W. Jiang, Y. Song, and S. G. Yang, *Controlled synthesis of ZnS nanocombs by self-evaporation using ZnS nanobelts as source and substrates*. Cryst. Eng. Comm., 2014, **14**, 708-712.
- <sup>51</sup> T. Y. Zhai, Z. J. Gu, Y. Ma, W. S. Yang, L. Y. Zhao, J. N. Yao, *Synthesis of ordered ZnS*

- nanotubes by MOCVD-template method. Mater. Chem. Phys.*, 2005, **12**, 281-284.
- <sup>52</sup> A. Schuchardt, T. Braniste, Y. K. Mishra, M. Deng, M. Mecklenburg, M. A. S. Kalceff, S. Raevschi, K. Schulte, L. Kienle, R. Adelung, and I. Tiginyanu, *Three-dimensional Aerographite-GaN hybrid networks: Single step fabrication of porous and mechanically flexible materials for multifunctional applications*. *Sci. Rep.*, 2015, **5**, 1-8.
- <sup>53</sup> D. F. Moore, Y. Ding, and Z. L. Wang, *Crystal Orientation-Ordered ZnS Nanowire Bundles*. *J. Am. Chem. Soc.*, 2004, **126**, 14372-14373.
- <sup>54</sup> R. Behrisch, *Sputtering by Particle bombardment*. Springer, 1981, **47**.
- <sup>55</sup> K. K. Zadeh, and B. Fry, *Nanotechnology-Enabled Sensors*. Springer, 2008.
- <sup>56</sup> R. Saravanan, and M. P. Rani, *Metal and Alloy Bonding – An Experimental Analysis, Charge Density in Metals and Alloys*. Springer, 2012.
- <sup>57</sup> Y. X. Wang, L. D. Zhang, C. H. Liang, G. Z. Wang, and X. S. Peng, *Catalytic growth and photoluminescence properties of semiconductor single-crystal ZnS nanowires*. *Chem. Phys. Lett.*, 2002, **357**, 314-318.
- <sup>58</sup> D. Denzler, M. Olschewski, and K. Sattler, *Luminescence studies of localized gap states in colloidal ZnS nanocrystals*. *J. Appl. Phys.*, 1998, **84**, 2841-2845.
- <sup>59</sup> F. H. Su, Z. L. Fang, B. S. Ma, K. Ding, and G. H. Li, *Temperature and pressure behavior of the emission bands from Mn-, Cu-, and Eu-doped ZnS nanocrystals*. *J. Appl. Phys.*, 2004, **95**, 3344-3349.
- <sup>60</sup> W. Q. Peng, G. W. Cong, S. C. Qu, and Z. G. Wang, *Synthesis and photoluminescence of ZnS:Cu nanoparticles*. *Opt. Mater.*, 2006, **29**, 313-317.

- <sup>61</sup> X. L. Wang, J. Y. Shi, Z. C. Feng, M. R. Li, and C. Li, *Visible emission characteristics from different defects of ZnS nanocrystals*. *Phys. Chem. Chem. Phys.*, 2011, **13**, 4715-4723.
- <sup>62</sup> L. Shi, K. Bao, J. Cao, and Y. Qian, *Growth and characterization of ZnS porous nanoribbon array constructed by connected nanocrystallinities*. *Cryst. Eng. Comm.*, 2009, **11**, 2308-2312.
- <sup>63</sup> N. Riehl, *Intrinsic defects and luminescence in II–VI-compounds*. *J. Lumin.*, 1981, **24/25**, 335-342.
- <sup>64</sup> H. Y. Wang, C. R. Wang, J. Xu, X. Liu, X. F. Xu, H. Z. Xing, L. J. Zhao, and X. S. Chen, *Different temperature dependence of excitonic and defect-related photoluminescence spectra in ZnS nanobelts and nanowires*. *J. Phys. D: Appl. Phys.*, 2012, **45**, 095301.

## 요 약 문

### 도핑 된 황화아연 나노구조체 합성

본 연구는 넓은 직접밴드갭을 가지는 대표적인 II-VI족 반도체 물질인 황화아연을 화학 기상 합성법을 통해 나노구조체의 합성하고 특성 분석에 대해 연구하였다. 황화아연 일차원 나노구조체 합성에 사용 된, 화학 기상 합성법은 열 이나 수송기체압력 과 같은 여러 반응 요인들을 통해 다양한 구조체를 합성할 수 있는 것으로 알려져 있다. 본 연구에서는 900, 1000, 1200 °C 다양한 합성온도에서 황화아연 구조체를 형성하며, 특정 온도 (900 °C) 에서 일차원 나노구조체가 형성 되는 것을 확인 할 수 있었다. 또한, 선행된 몇몇 연구들에서 전이금속이 도핑 된 황화아연 일차원 나노구조체에서 발광효율이 증가된 연구가 보고되었다. 그러므로, 본 연구에서는 구리와 망간 같은 전이금속과 황화아연을 900 °C 온도에서 합성함으로써, 전이금속이 도핑 된 황화아연 일차원 나노구조체를 합성하였다. 전자현미경을 통해, 도핑을 하지 않거나 구리가 도핑 된 일차원 나노구조체는 직경 약 30 ~ 60 nm 나노선이 형성되었음을 확인하였다. 반면에, 망간이 도핑 된 일차원 나노구조체는 성게모양의 계층구조와 칼모양의 구조체가 형성되었다. 음극선발광 측정법을 통해 가속 된 전자를 합성한 나노구조체에 입사시킴으로써, 황화아연 밴드갭 내 결함준위를 비롯 하여 불순물 준위를 확인하였다. 이로써, 성공적으로 전이금속이 도핑 된 황화아연 일차원 나노구조체를 합성할 수 있는 방법을 제시하며, 밴드갭 조절을 확인 했다는 연구 의의를 가진다.

핵심어: 황화아연, 일차원구조체, 도핑, 열 화학 기상 합성.